Astron. Astrophys. 283, 221–231 (1994)

ASTRONOMY AND ASTROPHYSICS

# Infrared lines as probes of solar magnetic features

## VII. On the nature of the Evershed effect in sunspots

**S.K. Solanki**[1], **C.A.P. Montavon**[1], **and W. Livingston**[2]

[1] Institute of Astronomy, ETH-Zentrum, CH-8092 Zürich, Switzerland
[2] National Solar Observatory, NOAO, * P.O.Box 26732, Tucson AZ 85726, USA

Received 18 May 1993 / Accepted 6 August 1993

**Abstract.** Stokes $I$ and $V$ profiles of 1.56$\mu$m lines are observed in sunspots and their surroundings near the solar limb. An analysis of these observations confirms that the magnetic field of the sunspots continues beyond their visible boundaries in the form of an extensive, low-lying (superpenumbral) canopy. We also find that the $V$ profiles, which are only formed above the canopy base, exhibit the Evershed effect with line shifts of 0.5–2 km s$^{-1}$, while the non-magnetic material below the canopy is at rest. The deduced geometry of the flow outside the sunspot suggests a resolution of the long standing dispute about the existence or not of an Evershed flow outside the visible sunspot. In addition, the low density of the gas above the canopy base implies that the mass flux in the magnetic canopy is much smaller ($\approx$ 10%) than the mass flux in the penumbra, where the 1.5 $\mu$m lines exhibit wavelength shifts of approximately 4 km s$^{-1}$. The present observations cast doubt on the standard interpretation of the photospheric Evershed effect in terms of a steady flow, in particular if it is driven by the siphon-flow mechanism.

**Key words:** sunspots – Sun: magnetic fields – Sun: activity – Sun: infrared

### 1. Introduction

The Evershed effect, i.e. systematic shifts and asymmetries of spectral lines in sunspot penumbrae (e.g. Evershed 1909; St. John 1913; Maltby 1964; Schröter 1965; Bhatnagar 1967), remains one of the more enigmatic phenomena related to sunspots. It is generally thought to be produced by a steady horizontal outflow of material in the photospheric layers of penumbrae (e.g. Meyer & Schmidt 1968; Montesinos & Thomas 1993; Thomas & Montesinos 1993). Recently, the discovery that the penumbral field is uncombed, i.e. organized in filaments of different inclination (Degenhardt & Wiehr 1991; Schmidt et al. 1992; Title et al. 1993; Lites et al. 1993) has provided a natural solution for the problem that the field lines are, on average, inclined while the flow is almost horizontal. Other problems associated with the Evershed effect still await a definitive solution. For example, a number of investigators present convincing observations suggesting that the Evershed effect ends abruptly at the sunspot boundary (e.g. Brekke & Maltby 1963; Wiehr et al. 1986; Wiehr & Balthasar 1989; Schröter et al. 1989; Title et al. 1992, 1993; Wiehr & Degenhardt 1992; cf. Fig. 5 of Johannesson 1993), while others argue equally convincingly that it continues beyond the visible sunspot boundary (e.g. Sheeley 1972; Küveler & Wiehr 1985; Dialetis et al. 1985; Alissandrakis et al. 1988; Dere et al. 1990; Börner & Kneer 1992).

Practically all previous observations have been restricted to visible spectra in unpolarized light. An exception is the investigation of McPherson et al. (1992), who detected Evershed line shifts at 1.56 $\mu$m, but did not analyse them in detail. Although Title et al. (1993) do analyse magnetograms, they determine line shifts from unpolarized filtergrams.

In the present paper we introduce two new aspects to the observational study of the Evershed effect; we analyze both Stokes $I$ and $V$ spectra and we investigate two lines at 1.56 $\mu$m in detail (namely the Landé $g$ = 3, Fe I 1.5648 $\mu$m and $g_{\rm eff}$ = 1.53, Fe I 1.5653 $\mu$m lines; see Solanki et al. 1992a, Paper II of the present series, for details). Due to the extremely high Zeeman sensitivity of the $g$ = 3 line (three times larger than of the most sensitive lines in the visible), it is possible to follow the magnetic field beyond the visible sunspot in the $V$ profiles and to search for the associated Evershed effect. Our data not only allow us to resolve the above-mentioned controversy, they also give us the opportunity to compare the mass flux in the penumbra and the superpenumbra. Another advantage of the chosen lines is their low height of formation in the penumbra, at a level at which the Evershed signal is largest.

The present observations are, however, restricted to a single slice through the sunspots and thus susceptible to asymmetries

*Send offprint requests to*: S.K. Solanki

* Operated by the Association of Universities for Research in Astronomy, Inc. (AURA) under cooperative agreement with the National Science Foundation

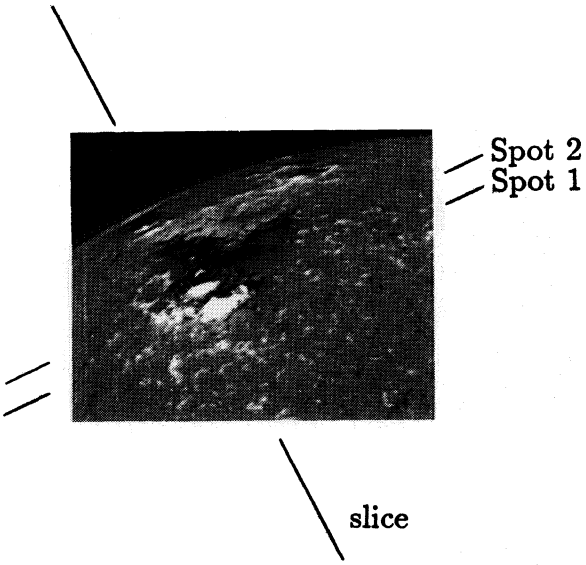


**Fig. 1.** Detail of the Kitt Peak magnetogram for 11th Oct, 1990 showing the observed sunspots and the direction of the slice

present in the Evershed flow field. Nevertheless, we do not expect such asymmetries to qualitatively affect our conclusions.

## 2. Observational data and method of analysis

Stokes $I \pm V$ of the two lines near 1.565 $\mu$m were obtained at a time of reasonably good seeing on 11th Oct, 1990 with the McMath telescope, vertical spectrograph and Baboquivari detector along a slice passing almost radially through two sunspots near the south-eastern solar limb ($\mu = \cos\theta$ varied between approximately 0.6 and 0.5 in the two sunspots). Both spots had the same polarity. They were leading spots of active region NOAA 6314. A magnetogram of the observed region, with the positions of the two sunspots and the direction of the slice indicated, is shown in Fig. 1.

We reduced the data by determining Stokes $I$ and $V$ from the observed spectra, removing the $I$ to $V$ cross-talk and Fourier smoothing the oversampled spectra. The wavelength was calibrated using a weak, telluric doublet at 15654.49Å and 15654.76Å (Bhatnagar, private communication, cf. Livingston & Wallace 1991). L. Wallace (private communication) has identified the two lines with water vapor transitions. Additional details on the instrumentation, observing procedure and data reduction are given by Livingston (1991) and in Paper II. Profiles were attributed to the umbra, penumbra or the non-spot surroundings by noting the position of the entrance aperture at the time of observation. Later we tested and confirmed this classification by considering the depth of the Fe I 15646.2Å line in the various spectra. The depth of this line increases almost linearly with decreasing temperature (except at very low temperatures, Montavon 1992; cf. Figs. 4–6 of Solanki et al. 1992b, hereafter called Paper V).

Stackplots of the observed Stokes $I$ and $V$ profiles are shown in Fig. 2. The profiles exhibit the usual features of these lines observed in sunspots, e.g. the very large splitting of the $g = 3$ line and the appearance of molecular blends to the $g_{\rm eff} = 1.53$ line in the umbra (spectra 5–10 and 16–19), or the presence of weak $V$ profiles well outside the visible boundary of the sunspot (e.g. spectra 23–27). In addition, there are some features which are due to the proximity of the limb, e.g., polarity inversions (profiles Nos. 10–12 in the limbside penumbra of the $\mu \approx 0.6$ spot, hereafter referred to as Spot 1, and profiles Nos. 18–19 in the umbra of the $\mu \approx 0.5$ spot, referred to as Spot 2) or highly asymmetric Stokes $I$ profiles in the penumbrae (see, e.g., the $g = 3$ line in spectra 15 and 21). This asymmetry is the most obvious sign of the Evershed effect. The positions of the polarity inversions are consistent with the measured field inclinations in sunspots (e.g. Kawakami 1983; Lites & Skumanich 1990; Adam 1990, Paper V; cf. the compilations by Solanki 1990 and Solanki & Schmidt 1993).

Cross-talk into Stokes $V$ due to the telescope is small, as can be judged by considering profile No. 18, at the apparent polarity inversion line in the sunspot umbra: Although the $V$ profile is small, it is antisymmetric. The other Stokes parameters are all symmetric and, for magnetic inclination angle $\gamma \approx 90°$, considerably larger than $V$ (particularly for the $g = 3$ line, see Paper II). A significant cross-talk would thus immediately introduce a large symmetric component into $V$. We estimate that the total uncompensated cross-talk into Stokes $V$ is less than 5% of the $\sqrt{Q^2 + U^2}$ signal.

We determine magnetic field strength and inclination, velocity shift and broadening, non-magnetic stray-light and temperature from these data using an inversion technique, i.e. by fitting the observed profiles with synthetic profiles that are solutions of the Unno-Rachkovsky equations in realistic atmospheres. The inversion code used here is similar to the ones described by Keller et al. (1990) and Ruiz Cobo & Del Toro Iniesta (1992) in that it makes no assumptions regarding the line formation (except for LTE) and can return complex stratifications of the velocity, magnetic vector, temperature, etc., if the correct parameterization is chosen. This is in contrast to the Milne-Eddington based models, which can either return only longitudinally averaged quantities (Skumanich & Lites 1987), or linear gradients (Landolfi 1987). Thus, for example, it is possible with the current code to carry out an inversion for a canopy-type field (horizontal field lines overlying a non-magnetic atmosphere) and determine the height of the canopy base. See Paper V and Solanki & Emonet (in preparation) for more on the inversion procedure. The largest difference compared to the inversion carried out in Paper V is that the temperature is now a free parameter of the inversion. Due to the presence of the 1.5653 $\mu$m line, the present data contain more information on the temperature than the data set analysed in Paper V (see Paper II).

The temperature, $T$, as a function of continuum optical depth, $\tau$, is determined by interpolating between the $T(\tau)$ values of two prescribed model atmospheres (see Emonet 1992 or Solanki & Emonet, in preparation, for details). After considering various model combinations we finally used only the quiet sun model of Maltby et al. (1986), which we call MALTQ, and their umbral model 'M', which we call MSPOTM. All the pro-

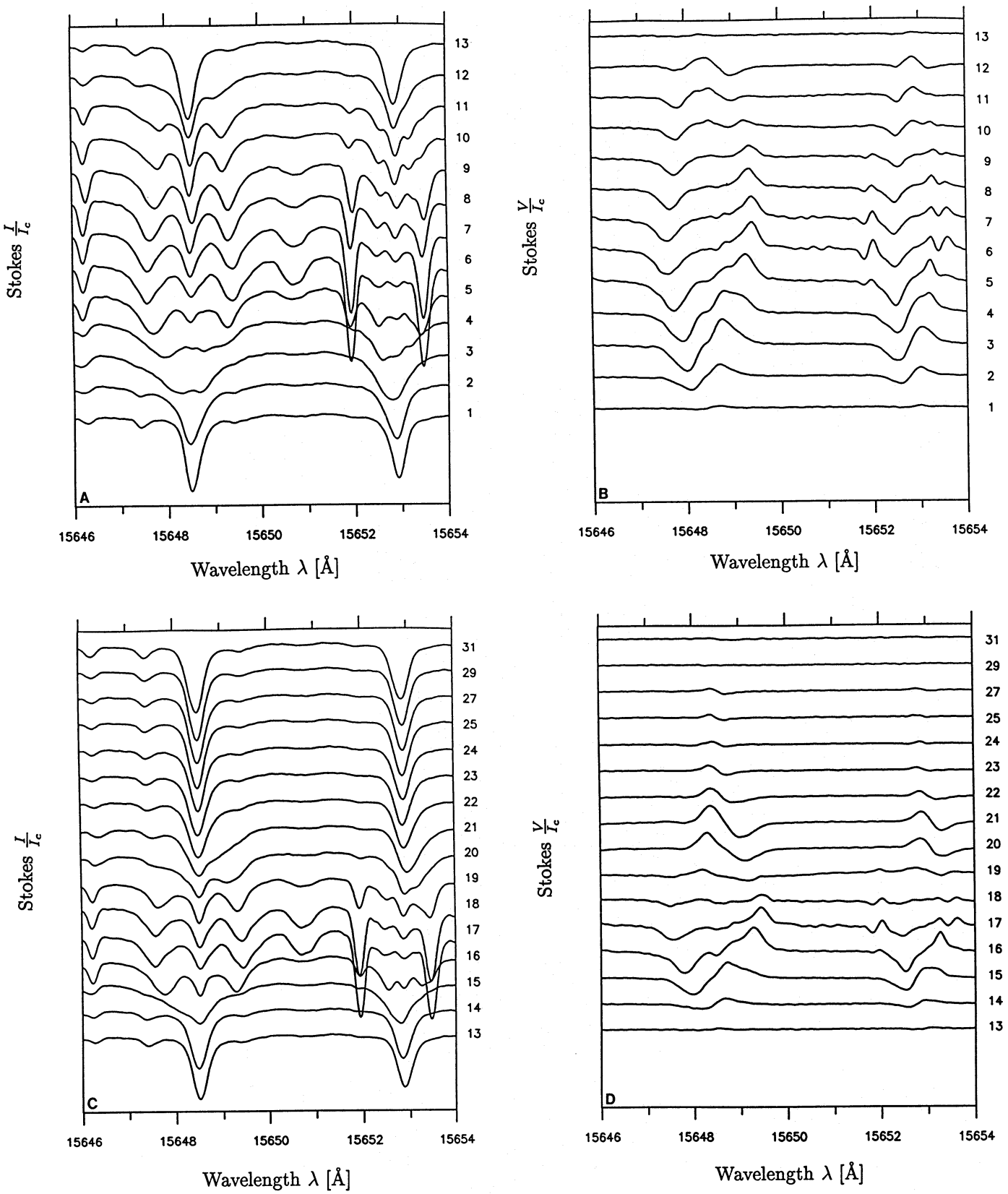


**Fig. 2a–d.** Observed Stokes $I$ and $V$ profiles of Fe I 15648Å and 15653Å along a slice lying perpendicular to the limb and passing through a sunspot at $\mu = \cos\theta \approx 0.6$ (**a** and **b**, called Spot 1) and $\mu \approx 0.5$ (**c** and **d**, called Spot 2). The uppermost spectra were obtained closest to the limb. Two consecutive spectra are separated by $\approx 3''$, except spectra Nos. 27, 29 and 31 which are separated by $6''$ from their neighbours

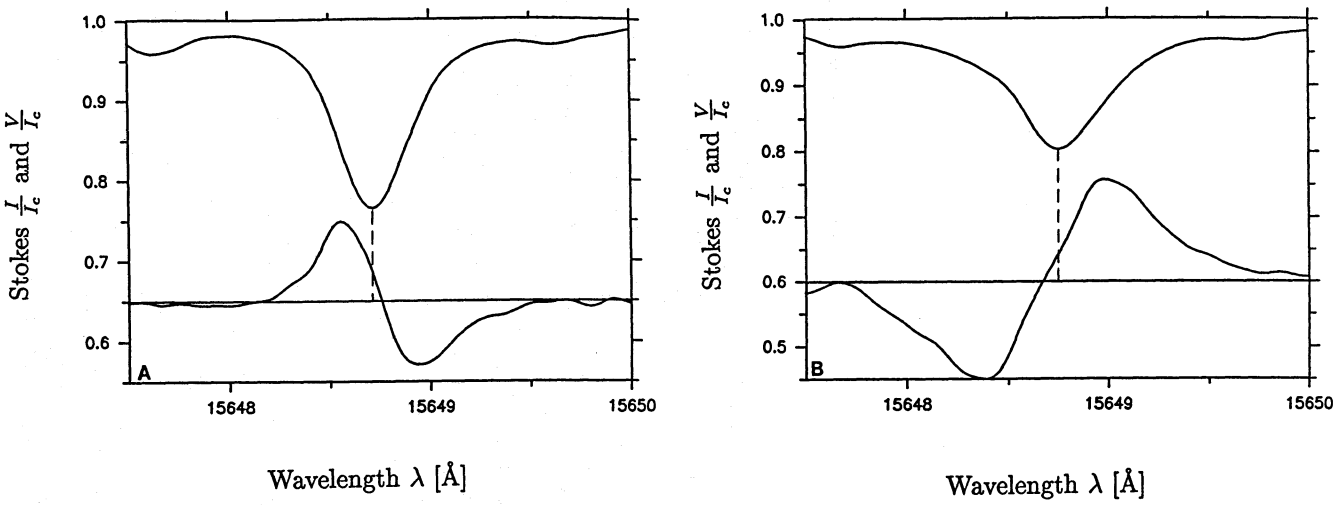


**Fig. 3a and b.** Stokes $I$ and $V$ profiles observed in the superpenumbral canopy of the sunspot; **a** on the limbward side, **b** on the discward side of the spot. Note the wavelength shift of the $V$ zero-crossing relative to the Stokes $I$ line core. The wavelength scale is not calibrated to an absolute value in this figure

files observed in the sunspots could be reasonably reproduced by linearly interpolating between the $T(\tau)$ of these two atmospheres and taking into account stray light.[1] In contrast, we found that the penumbral model of Ding & Fang (1989) gives line profiles near the limb whose depths and equivalent widths differed from the observed penumbral profiles by a factor of 2. The temperature gradient of this model between $\log\tau \approx -1$ and 0 is apparently too small.

## 3. Results of the profile fits

### *3.1. The superpenumbral canopy*

Most of the spectra observed outside the visible contours of the sunspot still show non-vanishing $V$ profiles. They have opposite polarities on the two sides of the spots and their amplitudes and Zeeman splittings decrease steadily with distance from the sunspot boundary (between the two spots no, or at the most very weak, $V$ profiles are visible). Following Paper V we interpret these profiles in terms of a canopy of horizontal magnetic field overlying a non-magnetic atmosphere. This interpretation is in line with the observations and analyses of Giovanelli (1980), Giovanelli & Jones (1982), Adams et al. (1993), Bruls et al. (1993, Paper VIII of the present series), Rüedi et al. (1993) and Lites (private communication 1993). All the currently available data point to the existence of extensive horizontal canopies, with a base in the middle/upper photosphere, surrounding sunspots. One of the most intriguing aspects of the superpenumbral data is the wavelength shift between the Stokes $I$ and $V$ profiles. Whereas the $I$ profiles have roughly the same (calibrated) wavelength in the limbward and discward *super*penumbrae, the $V$ profiles are red- and blueshifted, respectively. This relative shift is illustrated in Fig. 3. To analyze this and other aspects of these profiles more quantitatively, we apply our inversion code. We determine the following parameters: the field strength, $B$, the canopy base height, $z_c$, the velocity in the canopy, $v$, the macroturbulence, $\xi_{\rm mac}$, and the temperature $T(\tau_{1.6} = 0.1)$. We require that all parameters are the same for both lines. The origin of the height scale is the $\tau_{0.5\,\mu\rm m} = 1$ level in the quiet sun. The best-fit parameters are listed in Table 1. $r - r_p$ is the distance from the edge of the sunspot. Profile No. 24 is discussed separately later. The magnetic inclination angle to the line-of-sight, $\gamma$, is prescribed in the first step. It is later obtained from $\gamma'$, the inclination angle relative to the surface normal, which is determined iteratively following the procedure described in Paper V. This procedure demands that the lower boundary of the canopy is a field line. Since the canopy base height changes very slowly with $r - r_p$, $\gamma'$ close to 90° are obtained with great accuracy, much more accurately than direcly from the profiles. The velocity $v$ is assumed parallel to the field lines. Positive $v$ is directed away from the observer. When determining $v$, we assume that the $I$ profiles are at rest. If the $I$ profiles are everywhere shifted by the same amount due to, e.g., the granulation, then this shift will have to be subtracted from the $v$ values in Table 1. Note, however, that a constant Stokes $I$ shift leaves the *difference* in $v$ between the limb- and centre-side superpenumbrae unchanged and in no way affects the conclusions of this paper.

The canopy base height, $z_c$, is plotted vs. distance from the edge of the sunspot, $r - r_p$, in Fig. 4. The results for this parameter are in excellent agreement with those of Papers V and VIII. The temperature (not listed) is only certain to within ± 250 K, and scatters around the quiet-sun value within this range. Note that we have not included the effects of possible 'polarized stray light' from the sunspot into the superpenumba. The effect of this stray light is to increase the Stokes $V$ signal and thus lead to a too low canopy base in our analysis. Consequently, the $z_c$

[1] The rest of the atmospheric variables were self-consistently determined using the electron pressure and continuum absorption coefficient calculated by the routine package of Gustafsson (1973).

**Table 1.** Parameters derived from fits to the superpenumbral profiles

| Profile No. | $r - r_p$ (km) | $B$ (G) | $z_c$ (km) | $\gamma'$ (°) | $v$ (km s$^{-1}$) | $\xi_{mac}(V)$ (km s$^{-1}$) | $\xi_{mac}(I)$ (km s$^{-1}$) |
|---|---|---|---|---|---|---|---|
| | 500† | 100 | 50 | 0.5 | 0.4 | 0.5 | 0.5 |
| 1 | 7000 | 400 | 290 | 88.7 | −2.0 | 5.0 | 3.2 |
| 2 | 3500 | 1000 | 210 | 87.6 | −1.7 | 4.9 | 4.0 |
| 23 | 4200 | 500 | 270 | 86.0 | 0.8 | 3.7 | 3.3 |
| 24 | 8400 | 400 | 300 | 89.7 | 0.6 | 2.0 | 2.0 |
| | | 1000 | | 15 | * | 2.0 | 2.0 |
| 25 | 16800 | $\lesssim 300$ | 340 | 89.7 | 0.6 | 2.6 | 2.6 |
| 27 | 25200 | $\lesssim 300$ | 360 | 89.9 | 0.9 | 3.4 | 3.1 |

* A line-of-sight velocity of 3 km s$^{-1}$ is found, but this is probably a horizontal velocity, not aligned with the almost vertical field of the flux-tube component.

† The numbers in this row signify estimated errors.

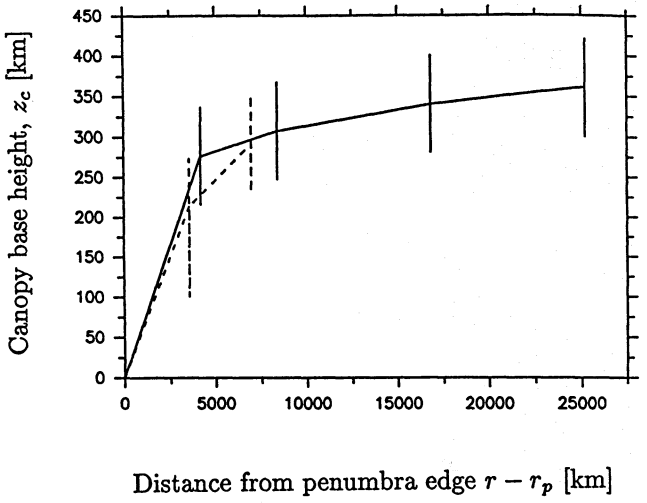


**Fig. 4.** Base height of the superpenumbral canopy, $z_c$, vs. distance from the outer penumbral boundary, $r - r_p$. Solid line: $z_c$ on the limbward side of spot 2, dashed line: $z_c$ on the discward side of spot 1

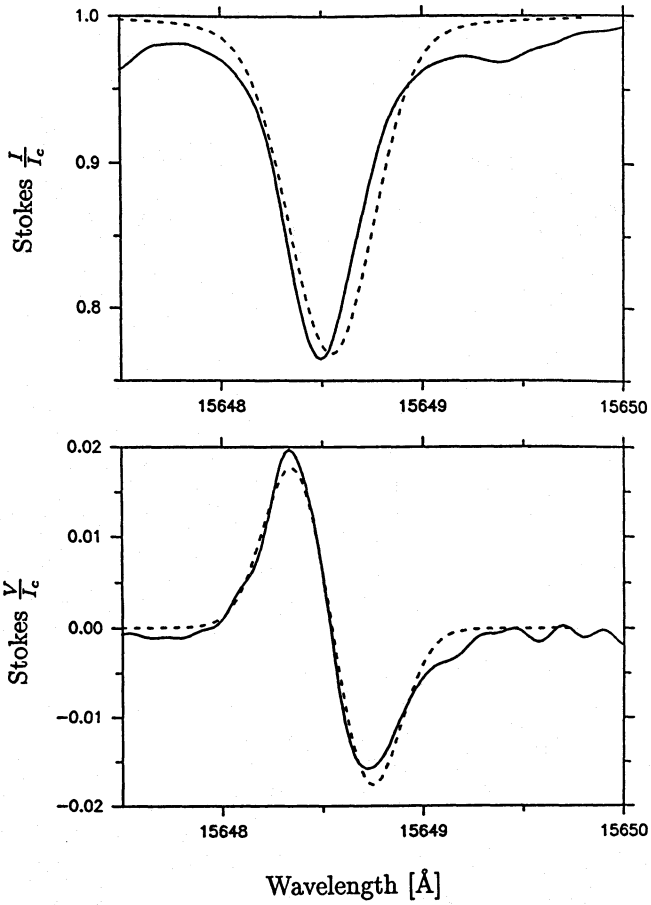


**Fig. 5.** Observed (solid) and synthetic (dashed) profiles of Fe I 15648Å in the superpenumbral canopy (same spectrum as in Fig. 3a). Upper frame: Stokes $I$, lower frame: Stokes $V$. The synthetic curves were calculated on the basis of the best-fit parameters to Stokes $V$

values for the profiles closest to the penumbrae (Nos. 2 and 23, and to a lesser extent 1 and 24) must be considered to be lower limits within the context of the simple model of the canopy used by us.

The parameters derived from Stokes $V$ generally also reproduce the corresponding $I$ profile, except for the line shift (and to a lesser extent the line width). Figure 5 shows observed (solid) and synthetic profiles calculated using the best-fit $V$ parameters. The figure confirms that the whole observed $V$ profile, and not just its core, is shifted relative to Stokes $I$.

The difference between the shifts of the $V$ and $I$ profiles is explained by noting that the contributions to the Stokes $I$ profiles of both lines peak well below the height of the canopy base, even at line centre. Consequently, the $I$ profile wavelengths respond dominantly to velocities below the canopy. The $V$ profiles, of course, are only formed in the magnetic portion of the atmosphere, i.e. above the canopy, so that the $V$ profile shifts reflect flows above the canopy base. For example, the Stokes $I$ contribution function calculated using the quiet sun model and a horizontal field of 400 G forming a canopy with a base at

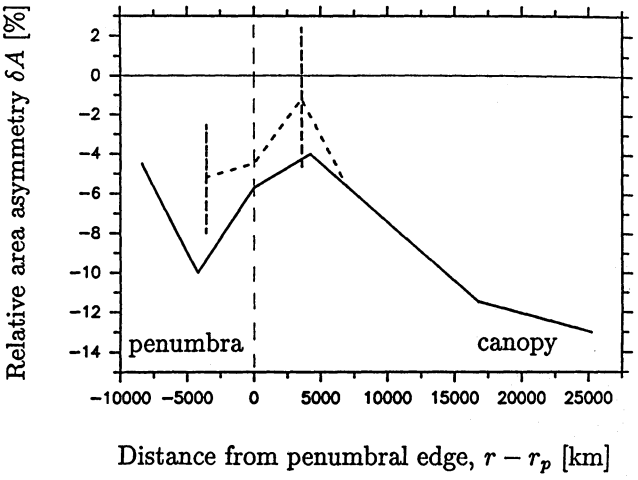


**Fig. 6.** Relative area asymmetry $\delta A$ of the Stokes $V$ profile of the $g = 3$ line vs. distance from the outer penumbral edge, $r - r_p$. Solid line: limbward side of spot 2 ($\mu \approx 0.5$), dashed line: discward side of spot 1 ($\mu \approx 0.6$). The 'error bars' indicate the difference between the $\delta A$ of two profiles obtained at the same spatial position

$z = 300$ km, peaks at $z = 150$ km in the line core, while the Stokes $V$ contribution function (at the wavelength of Stokes $V$ maximum) peaks at the canopy base and has a sharp lower edge.

Thus, our data exhibit an outflow in the superpenumbral magnetic canopy, but no such flow under the canopy. In summary, the Evershed flow continues at a speed of 0.5–2 km s$^{-1}$ beyond the outer boundary of the sunspot, but only above the base of the magnetic canopy.

Other signs of a velocity in the superpenumbral canopy are the large $\xi_{\rm mac}$ values (according to Table 1, the $V$ profiles often require more macroturbulent broadening than the $I$ profiles) and the $V$ asymmetry. In Fig. 6 we plot the relative area asymmetry of the $V$ profiles of the $g = 3$ line in the penumbra and the superpenumbra. Although the scatter is large, $\delta A = (A_b - A_r)/(A_b + A_r) < 0$ in the penumbra ($\delta A < 0$ implies that the red-lobe area, $A_r$, is larger than the blue-lobe area, $A_b$). It is gratifying to see that the sign of $\delta A$ is compatible with the broad-band circular polarization observed in sunspots (cf. Sánchez Almeida & Lites 1992; Solanki & Montavon 1993). The $V$ profiles in the canopy are also asymmetric, but the $\delta A$ values are less reliable. In particular, although $\delta A < 0$ for the limbward profiles, the sign of $\delta A$ is less clear for the profiles in the discward superpenumbra.

Finally, consider profile No. 24 on the limbward side of the spots. This profile distinctly shows the presence of two magnetic components and was fit manually using a horizontal canopy component (covering a fraction 0.9 of the surface; the parameters of this component are given on the first line referring to profile No. 24 in Table 1) and an almost vertical flux-tube component (covering the remaining fraction of the surface; second line in Table 1). The observed and synthetic profiles are compared in Fig. 7. The flux-tube component, which has the same polarity as the spots, exhibits a surprisingly large line-of-sight velocity of 3 km s$^{-1}$ directed towards the spots. Obviously this

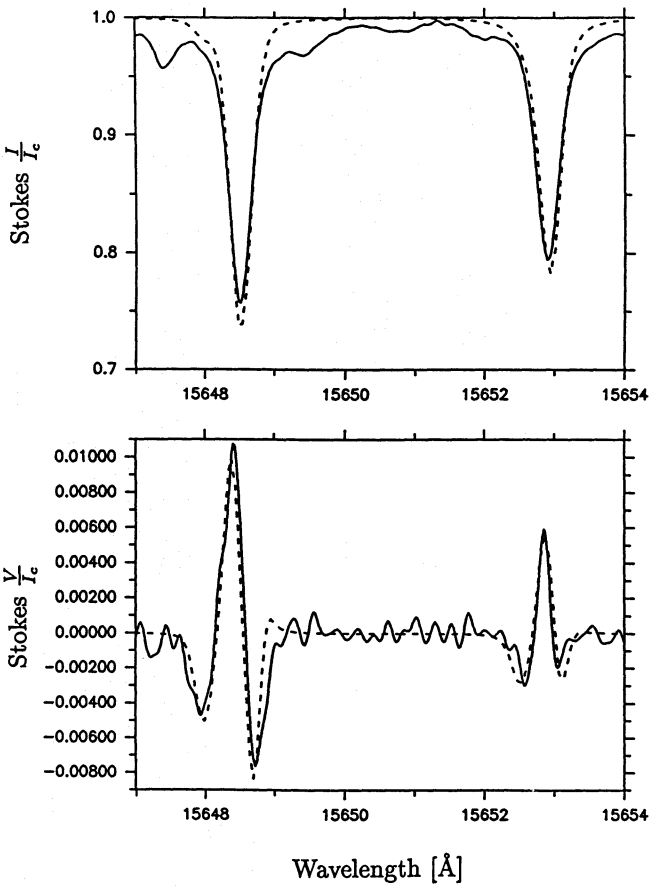


**Fig. 7.** Observed (solid) and synthetic (dashed) Stokes $I$ (upper frame) and $V$ (lower frame) profiles of the 1.56 $\mu$m lines (Spectrum No. 24). The synthetic profiles are based on a model with two magnetic components

velocity cannot be a continuation of the Evershed flow down the flux tube. Furthermore, it is unlikely that this velocity is field aligned, since the flux tube is almost perpendicular to the line-of-sight, so that a field-aligned flow would have to be supersonic.[2] We propose that the observed velocity is a horizontal velocity directed towards the sunspot. Magnetic features of the same polarity, flowing towards a sunspot are often associated with the growth of young sunspots (e.g. Vrabec 1974; Zwaan 1992). The flux tube parameters derived from spectrum No. 24 are less reliable than the other entries in Table 1.

### 3.2. *Penumbra*

A profile each from the limbward and discward penumbra of Spot 2 ($\mu \approx 0.5$) is plotted in Fig. 8. Note the relative shift between the spectra and the large asymmetry of the $g = 3$ Stokes $I$ profiles.

The profiles in the penumbra are fit by a 2-component model composed of a stray-light component, approximated by

[2] We derive $\gamma$ of the flux tube component by simultaneously fitting the $I$ and $V$ profiles and requiring that the filling factors of canopy and flux tube must together give unity.

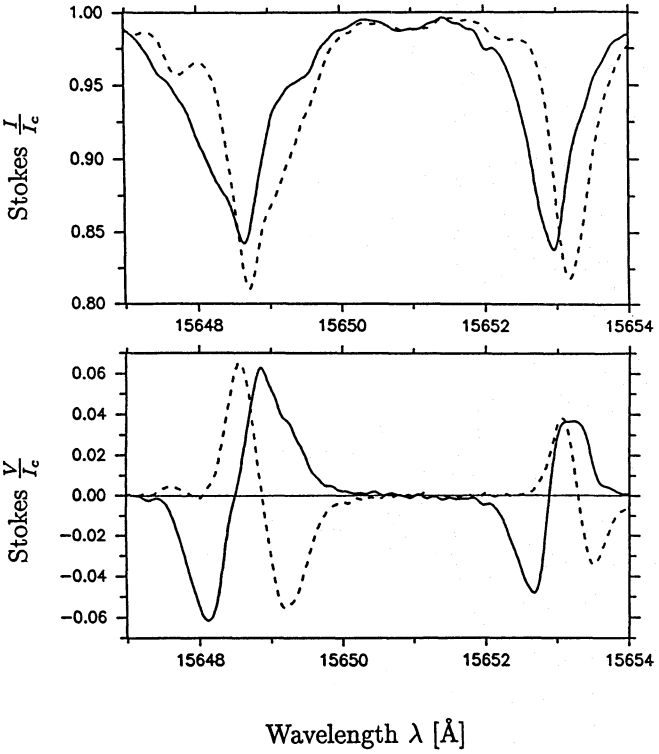


**Fig. 8.** Stokes $I$ (upper frame) and $V$ profiles (lower frame) observed in the penumbra. Solid curves: discward penumbra (spectrum No. 15), dashed curve: limbward penumbra (spectrum No. 21)

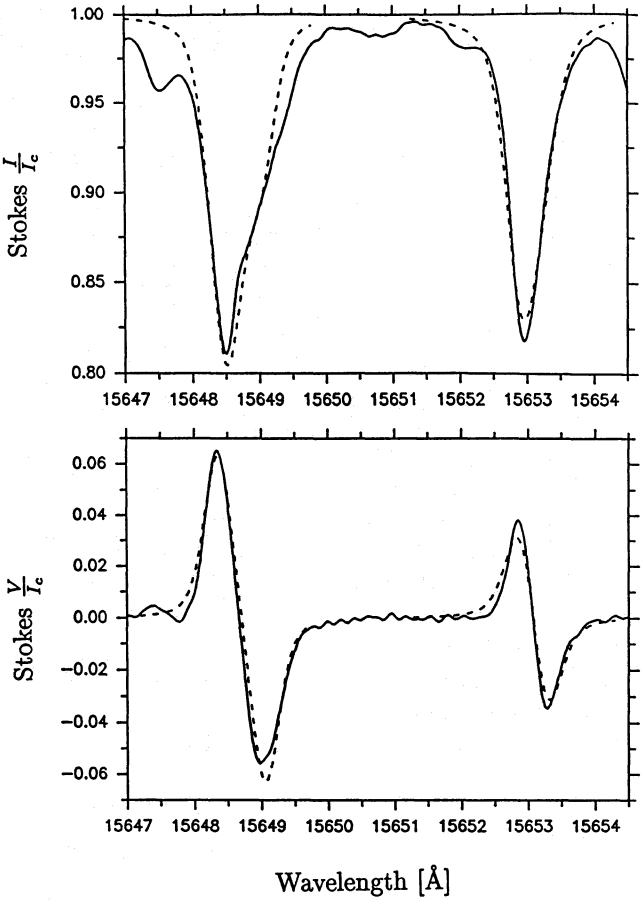


**Fig. 9.** Observed (solid) and best fit (dashed) line profiles. The observed spectrum is No. 21 from the limbward penumbra of Spot 2

the quiet-sun atmosphere, and a penumbral component. The free parameters for the inversion are $B, \gamma, \alpha, T, \xi_{\rm mac}$ and $v_{\rm LOS}$, where $\alpha$ is the filling factor of the magnetic component (i.e. $1-\alpha$ is a measure of the amount of unpolarized stray light) and $v_{\rm LOS}$ is the line-of-sight velocity restricted to the magnetic component. Best fits are obtained for 800 G $\lesssim B \lesssim$ 1600 G, 4800 K $\lesssim T$ ($\tau_{1.6}$ = 0.1) $\lesssim$ 4900 K, 40° $\lesssim \gamma \lesssim$ 175° (corresponding to 55° $\lesssim \gamma' \lesssim$ 85° for the negative polarity spots, under the assumption that the field is untwisted), $\xi_{\rm mac} \approx 4$ km s$^{-1}$ (excepting one profile which required 7.5 km s$^{-1}$), $\alpha \approx 0.65$–$0.80$ and 2 km s$^{-1} \lesssim |v_{\rm LOS}| \lesssim 4$ km s$^{-1}$.[3] For a horizontal Evershed flow (Maltby 1964; Johannesson 1993) this gives 2.5 km s$^{-1} \lesssim |v| \lesssim 4.5$ km s$^{-1}$, with an average value of 3.6 km s$^{-1}$.

Figure 9 shows, as an example, the fit to one of the observed spectra plotted in Fig. 8. The excess width of the observed $I$ profile of the $g$ = 3 line is due to the presence of a weak blend in each wing. The blend in the blue wing is easily identified as such in this figure, while the blend in the red wing is better visible in the solid profile in Fig. 8 (discward penumbra). The width of the $g$ = 3 Stokes $V$ profile lobes (which is not increased by blends), as well as the widths of the $I$ and $V$ profiles of the $g_{\rm eff}$ = 1.53 line are well reproduced, in support of the above conclusion.

The $B, T$ and $\gamma'$ values obtained from the inversion are unremarkable. The $\xi_{\rm mac}$ values are larger than obtained in Paper V close to disc centre (1–2 km s$^{-1}$), but are similar in magnitude to the broadening of the canopy profiles close to the sunspot (spectra 1, 2, 23, see Table 1). Velocity broadening in the horizontal direction is obviously larger than in the vertical direction (cf. Johannesson 1993).

The line shifts of the magnetic component relative to the quiet sun are large, considering the relatively low spatial resolution. In the visible typically measured velocities are 1–2 km s$^{-1}$at similar spatial resolution (e.g. Ichimoto 1987; Wiehr & Degenhardt 1992). The 1.56 $\mu$m lines are formed below the $\tau$ = 0.1 level, deeper than most lines in the visible.

These comparisons confirm the belief that the strength of the photospheric Evershed effect increases in magnitude with depth (e.g. St John 1913; Maltby 1964; Börner & Kneer 1992). Schröter et al. (1989), however, extrapolate from visible lines to $v(\tau = 1) \approx 2 - 2.5$ km s$^{-1}$, which is still smaller than the values we find. The unexpectedly large infrared value may be due to an increase in the vertical velocity gradient at the deepest

[3] Note that due to the considerable velocity shift of the true penumbral profiles relative to the 'stray-light' profiles it is possible to distinguish between $\alpha$ and $\gamma$, even though the $I$ profiles do not show a clear separation between $\pi$ and $\sigma$ components. For data showing no velocity shifts, on the other hand, $\alpha$ and $\gamma$ can only be separated if the spectral line is completely split (Paper V).

layers (Degenhardt 1993), but may also reflect horizontal inhomogeneities in the Evershed effect. For example, if the velocity is larger in dark fibrils, then we expect a larger total line shift in the infrared, since the dark fibrils give a greater contribution to the signal due to the decreased sensitivity of the Planck function to $T$ in the infrared. For the same reason, infrared lines are also expected to be broader. This may also explain the large macroturbulent velocity derived from the 1.56 $\mu$m data.

The large asymmetry of the Stokes $I$ profiles of the $g = 3$ line is *not* the result of a longitudinal velocity gradient. Test calculations showed that even a gradient as large as $dv/d\log\tau = 5$ km s$^{-1}$ produces a totally insufficient asymmetry of the $I$ profile (see Montavon 1992 for details). On the other hand, the introduction of an unshifted stray-light component into Stokes $I$ very easily produces the correct profile shapes, as indicated by Fig. 9. Thus, at least for the 1.56 $\mu$m lines, the asymmetry of Stokes $I$ is not due to the vertical gradient of the Evershed velocity, but rather to the presence of a stray-light component. This conclusion is supported by the fact that the $V$ profiles, whose shapes are insensitive to unpolarized stray light, are far less asymmetric than Stokes $I$.

We have also inverted the umbral spectral profiles, but the results are of no consequence for the conclusions of this paper. We, therefore, refrain from presenting any details.

## 4. Does the evershed flow continue beyond the visible penumbra?

As pointed out in the introduction, it is still controversial whether the Evershed effect stops at the visible boundary of the sunspot or continues beyond it. Some published observations show a sudden decrease of the line shift at the sunspot boundary, while others of equal quality show line shifts continuing well into the 'quiet' photosphere surrounding the sunspot. We believe that the key to resolving this discrepancy lies therein that the Evershed flow continues outside the sunspot only above the base of the magnetic canopy, as described in Sect. 3.1.

The previously published measurements were restricted to Stokes $I$, which is ill suited to decide this question. For example, a line with a low formation height detects no flow outside the sunspot (since the flow is present only above the canopy base), while a line formed at greater photospheric heights will detect a flow. Also, investigations measuring the shift of the line core are more likely to see an extension of the photospheric Evershed effect beyond the sunspot than those measuring the shift in the line flanks or those considering the Stokes $I$ line asymmetry. For strong lines this asymmetry changes sign at the sunspot boundary, mainly because the vertical velocity gradient seen by these lines changes sign. The apparent velocity amplitude increases with depth in the penumbra, but increases with height in the superpenumbra (a flow is seen only above the canopy). The asymmetry of lines with a low formation height also changes at $r_p$. Outside the penumbra these lines are formed mainly below the canopy, so that their asymmetry is due to the granulation and again differs from the asymmetry in the penumbra.

Consider two recent investigations coming to opposite results regarding the Evershed effect beyond the sunspot boundary. Wiehr & Degenhardt (1992) regarded the complete Evershed effect to be composed both of a line shift and line asymmetry. Due to the change in line asymmetry at the sunspot boundary they concluded that the Evershed effect stops there. Börner & Kneer (1992), on the other hand, observed numerous spectral lines, but only analyzed the core shift. They clearly saw an extension of the core shifts, particularly of the lines formed in the upper photosphere, and concluded that the Evershed effect does not disappear at the outer sunspot boundary. Our proposal that the Evershed effect continues outside sunspots only in the magnetic canopy is consistent with both observations.

## 5. Mass conservation

It is clear from Sects. 3.1 and 4 that the Evershed line shifts continue into the superpenumbral canopy. In this section we demonstrate that if the Evershed effect is due to a steady mass flow, then the mass flux directed outward through the canopy is only a small fraction of the mass flux in the penumbra.

The mass flowing outwards through a unit horizontal angle per time interval, $F_m$, can be expressed by the integral over height of the product of gas density, $\rho$, and (horizontal) velocity, $v$, over height,

$$F_m(r) = \Gamma(r) \int_{z_l(r)}^{z_u(r)} \rho(z,r)\, v_r(z,r)\, dz\ .$$

Here, $v_r$ is the radial component of the velocity (only it contributes to the net mass flux), $z_l$ and $z_u$ are the bottom and top boundaries of the height range containing the photospheric Evershed effect. $\Gamma \sim r/r_p$ is a factor taking into account the azimuthal expansion of the cross-sectional area of the flow with increasing $r/r_p$ [any changes in the vertical direction are already taken care of by $z_l(r)$ and $z_u(r)$]. Since we are only interested in the $F_m$ value at $r/r_p = 1.4$ relative to $F_m(r/r_p = 1)$, we simply use $\Gamma = r/r_p$.

To estimate $F_m$ within the penumbra we assume that $z_l$ is identical to the lowest atmospheric level to which the 1.56 $\mu$m lines are significantly sensitive. From test calculations we judge this level to be 50 km above $\tau_c = 1$; the two spectral lines are sensitive to velocity changes affected at this height. This level is not far below the height at which the $I$ and $V$ profiles obtain their largest contribution, which turns out to be $z = 80$ km for the $g = 3$ line at a typical penumbral temperature and a field strength of 1000 G. In fact, at $z = 50$ km the contribution function still has 75% of its maximum amplitude.

In the superpenumbra we set $z_l = z_c$, where $z_c$ is the height of the canopy base. Since the outflow is seen only in Stokes $V$ this is a reasonable lower limit. Recall that shifts in the Stokes $V$ zero-crossing can only be produced by flows in the magnetic part of the atmosphere (Grossmann-Doerth et al. 1988, 1989; Solanki 1989). We assume $z_u \approx 700$ km at all $r/r_p$, since observations referring to greater heights predominantly show an

inflow (e.g. Börner & Kneer 1992). The choice of $z_u$ is uncritical for the determination of $F_m$.

In the penumbra $\rho(z)$ is taken from a typical atmosphere producing good fits to penumbral profiles [$T(\tau = 1) = 4800$ K], while in the superpenumbra $\rho$ is taken from a standard quiet-sun model (Maltby et al. 1986).

Our best estimate is based on the following parameter values. Superpenumbral canopy (i.e. $r/r_p = 1.4$): $z_l = 270$ km, $z_u = 700$ km, $v = 1.4\,\mathrm{km\,s^{-1}}$ (independent of height) and $\Gamma = 1.4$ (values for a distance of $\approx 5000$ km from the boundary of the sunspot). Penumbra (i.e. $r/r_p = 1$): $z_l = 50$ km, $z_u = 700$ km, $\Gamma = 1$, $v = 3.5\,\mathrm{km\,s^{-1}}$ at $z = z_l$, decreasing linearly to 0 at $z_u$. The resulting $F_m$ ratio is:

$$\frac{F_m(r/r_p \approx 1.4)}{F_m(r/r_p \approx 1)} \approx 6\% .$$

A conservative upper limit on $F_m(r/r_p \approx 1.4)$ is obtained by assuming $z_l = 200$ km, $z_u = 1000$ km and $v = 2\,\mathrm{km\,s^{-1}}$ (again independent of height). Using these values we find

$$\frac{F_m(r/r_p \approx 1.4)}{F_m(r/r_p \approx 1)} \lesssim 13\% .$$

We see only one way of increasing the mass flux in the canopy, namely by lowering $z_c$. This is best achieved by introducing an azimuthal twist into the field. For an azimuthally twisted magnetic field the line-of-sight velocity becomes smaller than the true velocity and, of particular importance, the $V$ amplitude is also decreased. Judging from vector magnetograms (e.g. Adams et al. 1993) and $H_\alpha$ images, azimuthal angles of the magnetic vector as large as 45° to the radial direction are rarely reached at $r/r_p < 2$. Assuming a twist of 45° at $r/r_p \approx 1.4$, while keeping the twist = 0° at $r/r_p = 1$ we still obtain an increase in $F_m(r/r_p = 1.4)$ of less than a factor of 1.5, so that our conservative upper limit becomes:

$$\frac{F_m(r/r_p = 1.4)}{F_m(r/r_p = 1)} \lesssim 20\% .$$

For our best estimate we use a more typical value of $\phi \approx 10 - 30°$, which is also consistent with the results of e.g. Alissandrakis et al. (1988) and Dere et al. (1990), who find that the gas propagates almost radially even at $r/r_p \approx 1.5$. Their conclusion is supported by the data of Börner & Kneer (1992). Note that the velocity in the canopy which we measure is of the same magnitude as that observed by the above investigators, which supports the absence of a sizeable twist in our data set as well. For our best estimate we finally obtain

$$\frac{F_m(r/r_p = 1.4)}{F_m(r/r_p = 1)} \approx 6 - 8\% .$$

One uncertainty is caused by the unknown azimuthal twist of the sunspot's magnetic field. A larger twist than assumed should raise the limit on $F_m(r/r_p = 1.4)/F_m(r/r_p = 1)$. On the other hand, we have neglected the polarized stray light from the sunspot itself. The inclusion of this stray light should raise the derived $z_c$ and thus lower $F_m(r/r_p = 1.4)/F_m(r/r_p = 1)$.

## 6. Nature of the evershed effect: Is it due to a steady flow?

In Sect. 5 we saw that if we interpret the Evershed effect as a steady flow in a simple geometry, then we have difficulty conserving mass. Before drawing any conclusions on the nature of the Evershed effect we consider two possible scenarios for reconciling a stationary flow with the present observations and mass conservation.

a) *Return flux*: Could the matter flow mainly along field lines that disappear below the surface inside or less than $3'' - 4''$ outside the outer penumbral boundary? 1.5 $\mu$m and 12 $\mu$m spectra can follow the field well beyond the visible sunspot. They provide no evidence for return flux in the immediate surroundings of a sunspot (Paper V, Hewagama et al. 1993; see Bruls et al. 1993 for a more detailed analysis of their spectra). Solanki & Schmidt (1993) support this conclusion, based on a more careful analysis of the 1.5 $\mu$m data. Similarly, the high-resolution images of Title et al. (1993) and spectra of Lites et al. (1993) show no sign of systematic return flux within the penumbra or just outside it.
Let us assume, against the evidence, that some magnetic flux does return to the solar interiour within the penumbra. Could such a geometry support a stationary Evershed flow? The siphon flow mechanism is usually invoked to explain the Evershed effect in terms of stationary flows (e.g. Meyer & Schmidt 1968; Degenhardt 1991; Montesinos & Thomas 1993; Thomas & Montesinos 1993). Under realistic conditions (i.e. for finite viscosity) this mechanism always predicts a flow along a loop from the footpoint of smaller field strength to the footpoint with larger field strength. Since the field strength in the penumbra drops rapidly outwards at roughly equal gravitational potential (Wilson & Cannon 1968; Wittmann & Schröter 1969, Solanki et al. 1993, Paper VI of the present series), for purely penumbral loops these models predict a flow directed towards the umbra, contrary to the observations.

b) *Field-free channels*: Could the flow be concentrated in field-free channels within the penumbra? This scenario, if correct, would provide an elegant solution to the problem at hand, since, upon reaching the outer edge of the visible penumbra, the outflowing material can simply spill out into the non-magnetic atmosphere and disappear into the solar interiour. In Paper V we determined that in the lower layers of the penumbra at the most 5% of the gas is field free. Deming et al. (1991) and Hewagama et al. (1993) set even tighter limits on the amount of field-free gas in the upper photospheric layers of penumbrae. These limits imply that the entire Evershed flow would have to be concentrated into less than 5% of the available volume, so that in order to produce a spatially averaged Evershed velocity of 1 km $\mathrm{s^{-1}}$, the true velocity within the field-free channels would have

to be greater than 20 km $s^{-1}$. A velocity so far in excess of the sound speed does not appear likely.

In addition, as Figs. 8 and 9 clearly demonstrate, the Stokes $V$ profiles exhibit shifts that are entirely consistent with the Stokes $I$ shifts. Since $V$ profile zero-crossing shifts only result from mass motions in a magnetized gas, this observation rules out that the Evershed effect is due to flows in field-free channels.

Neither of the scenarios discussed above appears to provide a satisfactory solution to the mass conservation problem. Consequently, a steady outward flow of matter faces grave problems in explaining the current observations of penumbrae without conflicting with conservation principles. The most straightforward alternative is to consider the Evershed effect to be due to a time-dependent velocity or to convective motions. Candidates for such motions are: Convection, either in the form of rolls (e.g. Danielson 1961) or of flux-tube exchange (Jahn 1992), unsteady flows along 'fallen flux tubes' (Wentzel 1992), or waves (Maltby & Eriksen 1967; Bünte et al. 1993). The mechanisms based on waves and convective motions involve no net mass transport and depend on temperature-velocity or pressure-velocity correlations to produce line shifts and asymmetries. None of these three mechanisms has been sufficiently analyzed and so far observations have not been able to distinguish between them.

## 7. Conclusions

We have analysed Stokes $I$ and $V$ spectra of lines at 1.56 $\mu$m observed in and around sunspots located near the solar limb. These lines exhibit the Evershed effect in both the sunspot penumbrae and the superpenumbral canopies. The most important result is that although the line shifts associated with the Evershed effect are clearly seen beyond the visible outlines of the sunspot, they are restricted to heights lying above the base of the magnetic canopy. Since the gas density at these heights is an order of magnitude smaller than at the height at which the largest Evershed shifts are measured in the penumbra, the mass flux in the canopy is also an order of magnitude smaller than in the penumbra (under the assumption that the Evershed effect is caused by a steady outflow of matter).

Thus, the current limits set by observations cast serious doubt on steady flows as the source of the Evershed effect. In particular the siphon flow mechanism does not appear to satisfy the observational constraints. Nevertheless, we feel that it is imporant to carry out further observations with the highest possible spatial resolution in different spectral lines in the visible and at 1.5 $\mu$m to look for any loopholes in the current observational material that may allow outflowing mass to return to the solar interiour unnoticed. One quantity which must be better constrained in future investigations is the azimuthal component of the magnetic field in the superpenumbra. Improved modelling of the canopy should also be aimed at. In parallel, alternatives to the current steady-flow interpretation should be explored.

*Acknowledgements.* We thank Prof. A. Bhatnagar for pointing out the presence of a telluric line in the observed wavelength range, and Prof. E.H. Schröter and Dr. D. Degenhardt for helpful discussions on the Evershed effect and siphon flows, respectively.

## References

Adam M.G., 1990, Sol. Phys. 125, 37
Adams M., Solanki S.K., Hagyard M., Moore R.L., 1993, Sol. Phys. in press
Alissandrakis C.E., Dialetis D., Mein P., Schmieder B., Simon G., 1988, A&A 201, 339
Bhatnagar A., 1967, *Kodaikanal Obs. Bull.* **180**, A13
Börner P., Kneer F., 1992, A&A 255, 307
Brekke K., Maltby P., 1963, Ann. d'Astrophys. 26, 383
Bruls J.H.M.J., Solanki S.K., Carlsson M., Rutten R.J., 1993, A&A submitted (Paper VIII)
Bünte M., Darconza G., Solanki S.K., 1993, A&A 274, 478
Danielson R.E., 1961, ApJ 134, 289
Degenhardt D., 1991, A&A 248, 637
Degenhardt D., 1993, A&A in press
Degenhardt D., Wiehr E., 1991, A&A 252, 821
Deming D., Hewagama T., Jennings D.E., Wiedemann G., 1991, in Solar Polarimetry, L.J. November (Ed.), National Solar Obs., Sunspot, NM, p. 341
Dere K.P., Schmieder B., Alissandrakis C.E., 1990, A&A 233, 207
Dialetis D., Mein P., Alissandrakis C.E., 1985, A&A 147, 93
Ding M.D., Fang C., 1989, A&A 225, 204
Emonet Th., 1992, Diplomarbeit, ETH, Zürich
Evershed J., 1909, MNRAS 69, 454
Giovanelli R.G., 1980, Sol. Phys. 68, 49
Giovanelli R.G., Jones H.P., 1982, Sol. Phys. 79, 267
Grossmann-Doerth U., Schüssler M., Solanki S.K., 1988, A&A 206, L37
Grossmann-Doerth U., Schüssler M., Solanki S.K., 1989, A&A 221, 338
Gustafsson B., 1973, *Uppsala Astron. Obs. Ann.* **5**, No. 6
Hewagama T., Deming D., Jennings D.E., Osherovich V., Wiedemann G., Zipoy D., Mickey D.L., Garcia H., 1993, ApJS 86
Ichimoto K., 1987, PASJ 39, 329
K. Jahn, 1992, in Sunspots: Theory and Observations, J.H. Thomas, N.O. Weiss (Eds.), Kluwer, Dordrecht, p. 139
Johannesson A., 1993, A&A 273, 633
Kawakami H., 1983, PASJ 35, 459
Keller C.U., Solanki S.K., Steiner O., Stenflo J.O., 1990, A&A 233, 583
Küveler G., Wiehr E., 1985, A&A 142 205
Landolfi M., 1987, Sol. Phys. 109, 287
Lites B.W., Skumanich A., 1990, ApJ 348, 747
Lites B.W., Elmore D.F., Tomczyk S., Seagraves P., Skumanich A., Streander K.V.: 1993, in The Magnetic and Velocity Fields of Solar Active Regions, H. Zirin (Ed.), Astron. Soc. Pacific Conf. Ser., IAU Coll. 141, 173
Livingston W., 1991, in Solar Polarimetry, L. November (Ed.), National Solar Obs., Sunspot, NM, p. 356
Livingston W., Wallace L., 1991, *An Atlas of the Solar Spectrum in the Infrared from 1850 to 9000 $cm^{-1}$ (1.1 to 5.4 $\mu$m)*, NSO Technical Report # 91-001, National Solar Obs., Tucson, AZ
Maltby P., 1964, *Astrophys. Norvegica* **8**, 205
Maltby P., Eriksen G., 1967, Sol. Phys. 2, 249
Maltby P., Avrett E.H., Carlsson M., Kjeldseth-Moe O., Kurucz R.L., Loeser R., 1986, ApJ 306, 284

McPherson M.R., Lin H., Kuhn J.R., 1992, Sol. Phys. 139, 255
Meyer F., Schmidt H.U., 1968, *Z. Angew. Math. Mech.* **48**, 218
Montavon C., 1992, Diplomarbeit, ETH Zürich
Montesinos B., Thomas J.H., 1993, ApJ 402, 314
Rüedi I., Solanki S.K., Livingston W., 1993, in Solar Magnetic Fields, M. Schüssler, W. Schmidt (Eds.), Cambridge University Press, in press
Ruiz Cobo B., Del Toro Iniesta J.C., 1992, ApJ 398, 375
Sánchez Almeida J., Lites B.W., 1992, ApJ 398, 359
Schmidt W., Hofmann A., Balthasar H., Tarbell T.D., Frank Z.A., 1992, A&A 264, L27
Schröter E.H., 1965, *Z. Astrophys.* **62**, 228
Schröter E.H., Kentischer T., Münzer H., 1989, in High Spatial Resolution Solar Observations, O. von der Lühe (Ed.), National Solar Obs., Sunspot, NM, p. 299
Sheeley N.R., Jr., 1972, Sol. Phys. 25, 98
Skumanich A., Lites B.W., 1987, ApJ 322, 473
Solanki S.K., 1989, A&A 224, 225
Solanki S.K., 1990, in *Solar Photosphere: Structure, Convection and Magnetic Fields*, J.O Stenflo (Ed.), *IAU Symp.* **138**, 103
Solanki S.K., Montavon C.A.P., 1992, A&A 275, 283
Solanki S.K., Schmidt H.U., 1993, A&A 267, 287
Solanki S.K., Rüedi I., Livingston W., 1992a, A&A 263, 312 (Paper II)
Solanki S.K., Rüedi I., Livingston W., 1992b, A&A 263, 339 (Paper V)
Solanki S.K., Walther U., Livingston W., 1993, A&A in press (Paper VI)
St. John C.E., 1913, ApJ 37, 322
Thomas J.H., Montesinos B., 1993, ApJ 407, 398
Title A.M., Frank Z.A., Shine R.A., Tarbell T.D., Topka K.P., Scharmer G., Schmidt W., 1992, in Sunspots: Theory and Observations, J.H. Thomas, N.O. Weiss (Eds.), Kluwer, Dordrecht, p. 195
Title A.M., Frank Z.A., Shine R.A., Tarbell T.D., Topka K.P., Scharmer G., Schmidt W., 1993, ApJ 403, 780
Vrabec D., 1974, in Chromospheric Fine Structure, R.G. Athay (Ed.), Reidel, Dordrecht, IAU Symp. 56, 201
Wentzel D.G., 1992, ApJ 388, 211
Wiehr E., Balthasar H., 1989, A&A 208, 303
Wiehr E., Degenhardt D., 1992, A&A 259, 313
Wiehr E., Stellmacher G., Knölker M., Grosser H., 1986, A&A 155, 402
Wilson P.R., Cannon C.J., 1968, Sol. Phys. 4, 3
Wittmann A., Schröter E.H., 1969, Sol. Phys. 10, 357
Zwaan C., 1992, in Sunspots: Theory and Observations, J.H. Thomas, N.O. Weiss (Eds.), Kluwer, Dordrecht, p. 75

This article was processed by the author using Springer-Verlag TEX A&A macro package 1992.